Modified embedded-atom method interatomic potentials for the Mg-Al alloy system

B. Jelinek,[1,2] J. Houze,[1,2] Sungho Kim,[1,2] M. F. Horstemeyer,[3,2] M. I. Baskes,[4] and Seong-Gon Kim[1,2]

[1] Department of Physics and Astronomy, Mississippi State University, MS State, Mississippi 39762, USA
[2] Center for Advanced Vehicular Systems, Mississippi State University, Mississippi State, MS 39762, USA
[3] Department of Mechanical Engineering, Mississippi State University, MS State, Mississippi 39762
[4] Los Alamos National Laboratory, MST-8, MS G755, Los Alamos, NM 87545

(Dated: April 15, 2024)

We developed new modified embedded-atom method (MEAM) interatomic potentials for the Mg-Al alloy system using a first-principles method based on density functional theory (DFT). The materials parameters, such as the cohesive energy, equilibrium atomic volume, and bulk modulus, were used to determine the MEAM parameters. Face-centered cubic, hexagonal close packed, and cubic rock salt structures were used as the reference structures for Al, Mg, and MgAl, respectively. The applicability of the new MEAM potentials to atomistic simulations for investigating Mg-Al alloys was demonstrated by performing simulations on Mg and Al atoms in a variety of geometries. The new MEAM potentials were used to calculate the adsorption energies of Al and Mg atoms on Al (111) and Mg (0001) surfaces. The formation energies and geometries of various point defects, such as vacancies, interstitial defects and substitutional defects, were also calculated. We found that the new MEAM potentials give a better overall agreement with DFT calculations and experiments when compared against the previously published MEAM potentials.

PACS numbers: 61.50.Lt, 62.20.Dc, 61.72.Ji, 68.35.-p

I. INTRODUCTION

Magnesium alloys are becoming increasingly important in many technological areas, including aerospace and automotive industries. The usage of magnesium die castings, for example, is increasing in the automotive industry[1,2,3] due to the lower mass densities of magnesium alloys compared with steel and aluminum, higher temperature capabilities and improved crash-worthiness over plastics. The primary magnesium alloys for die-casting applications are the magnesium-aluminum alloys such as AM 50 and AM 60B[4,5,6].

To meet the industrial demand for high-strength lightweight magnesium alloys, it is essential to obtain detailed understanding of the effect of individual alloying elements on the properties of magnesium alloys, especially among the main constituent elements, Mg and Al. The alloying elements can form interstitial or substitutional defects, or can precipitate into small particles creating complex interface structures. The interactions between these alloying elements need to be investigated using atomistic simulation techniques such as molecular dynamics or Monte Carlo simulations. These atomistic simulations require accurate atomic interaction potentials to compute the total energy of the system. First-principles calculations certainly can provide the most reliable interatomic potentials. However, realistic simulations of alloy systems often require a number of atoms that renders these methods impractical – they either require too much computer memory or take too long to be completed in a reasonable amount of time. One alternative is to use (semi-)empirical interaction potentials that can be evaluated efficiently, so that the atomistic approaches that use them can, in certain cases, handle systems with more than a million atoms.

There are two additional essential features that are expected from a useful semiempirical approach besides its efficiency: reliability and flexibility. A reliable interatomic potential would accurately reproduce various fundamental physical properties of the relevant element or alloy, such as elastic, structural, and thermal properties. Reliability also includes transferability. A transferable interatomic potential would perform reasonably well even under circumstances that were not used during its construction phase. A flexible semiempirical approach can represent interaction potentials among a wide variety of elements and their alloys using a common mathematical formalism. The modified embedded-atom method (MEAM) potential proposed by Baskes et al. was the first semiempirical atomic potential using a single formalism for fcc, bcc, hcp, diamond-structured materials and even gaseous elements, in good agreement with experiments or first-principles calculations[7,8,9,10]. The MEAM is an extension of the embedded-atom method (EAM)[11,12] to include angular forces. The EAM was able to reproduce physical properties of many metals and impurities. The EAM was applied to hydrogen embrittlement in nickel[13], and to nickel and palladium with hydrogen[12]. Cherne et al. made a careful comparison of MEAM and EAM calculations in a liquid nickel system[14].

Atomistic simulations of a wide range of elements and alloys have been performed using the MEAM potentials. Baskes[7] first proposed the MEAM method to obtain realistic shear behavior for silicon. Baskes et al.[8] then provided the MEAM model of silicon, germanium and their alloys. The MEAM was also applied to 26 single elements[9] and to silicon-nickel alloys and interfaces[15]. Gall et al.[16] used the MEAM to model the tensile debonding of an aluminum-silicon interface. Lee and Baskes[17] improved the MEAM to account for the second

nearest-neighbor interactions. Also, Huang et al.[18] used the MEAM and two other potentials to determine defect energetics in beta-SiC. The MEAM parameters for a nickel and molybdenum-silicon system were determined by Baskes[19,20]. Recently, an effort has been made by Lee et al.[21] to create the MEAM potentials for Cu, Ag, Au, Ni, Pd, Pt, Al, and Pb, based on the first and the second nearest-neighbor MEAM. A new analytic modified embedded-atom method (AMEAM) many-body potential was also proposed and applied to 17 hcp metals, including Mg[22,23]. For the Mg-Al alloy system, a set of EAM potentials have been developed using the "force matching" method by Liu et al.[24]. The structural properties of various polytypes of carbon were described using a MEAM potential[25]. Finally, Potirniche et al.[26] used the MEAM to analyze damage evolution in a single crystal nickel.

The purpose of the present work is to develop the MEAM potentials for aluminum, magnesium, and their alloy systems based on first-principles calculations using density-functional theory (DFT). Energy calculations and geometry optimizations of various structures were performed within the local-density approximation (LDA)[27,28] using ultrasoft pseudopotentials[29,30,31]. The cross pair potential was constructed by fitting elastic properties from DFT calculations for aluminum and magnesium in the B1 reference structure. First, the equilibrium lattice parameter, cohesive energy, bulk modulus, trigonal and tetragonal shear moduli were determined from DFT calculations. The pair potential was then constructed to fit the equilibrium volume and bulk modulus from ab initio calculations. Moreover, an effort has been made to match the sign of trigonal and tetragonal shear moduli. The new MEAM potentials were used to find the most energetically favorable structures for single elements and their pair combinations. The resulting energy-volume curves reasonably match the ab initio calculations. Satisfactory agreement of vacancy formation and stacking fault energies from DFT and MEAM calculations was found. Throughout this paper, the performance of our new potentials will be compared with the previously published MEAM potentials[21,22,24].

The paper is organized in the following manner. In Sec. II, we give a brief review of the MEAM. In Sec. III, the procedure for determination of the MEAM parameters is presented along with the new MEAM interatomic potential parameters. Validation of the newly developed MEAM potentials is presented in Sec. IV. Different bulk structures, surface defects, and point defects calculations were performed and compared with DFT calculations and experiments. Finally, in Sec. V, we discuss and summarize the results.

II. MEAM THEORY

The total energy E of a system of atoms in the MEAM[32] is approximated as the sum of the atomic energies

$$E = \sum_i E_i : \tag{1}$$

The energy of atom i consists of the embedding energy and the pair potential terms:

$$E_i = F_i(\rho_i) + \frac{1}{2}\sum_{j \neq i} \phi_{ij}(r_{ij}) : \tag{2}$$

F is the embedding function, ρ_i is the background electron density at the site of atom i, and $\phi_{ij}(r_{ij})$ is the pair potential between atoms i and j separated by a distance r_{ij}. The embedding energy $F_i(\rho_i)$ represents the energy cost to insert atom i at a site where the background electron density is ρ_i. The embedding energy is given in the form

$$F_i(\rho_i) = A_i E_i^0 \rho_i \ln(\rho_i); \tag{3}$$

where the sublimation energy E_i^0 and parameter A_i depend on the element type of atom i. The background electron density ρ_i is given by

$$\rho_i = \frac{\rho_i^{(0)}}{\rho_i^0} G(\Gamma_i); \tag{4}$$

where

$$\Gamma_i = \sum_{k=1}^{3} t_i^{(k)} \left(\frac{\rho_i^{(k)}}{\rho_i^{(0)}} \right)^2 \tag{5}$$

and

$$G(\Gamma) = \sqrt{1+\Gamma}\,. \tag{6}$$

The zeroth and higher order densities, $\rho_i^{(0)}$, $\rho_i^{(1)}$, $\rho_i^{(2)}$, and $\rho_i^{(3)}$ are given in Eqs. (9). The composition-dependent electron density scaling ρ_i^0 is given by

$$\rho_i^0 = \rho_{i0} Z_{i0} G\left(\Gamma_i^{ref}\right); \tag{7}$$

where ρ_{i0} is an element-dependent density scaling, Z_{i0} is the first nearest-neighbor coordination of the reference system, and Γ_i^{ref} is given by

$$\Gamma_i^{ref} = \frac{1}{Z_{i0}^2} \sum_{k=1}^{3} t_i^{(k)} s_i^{(k)}; \tag{8}$$

where $s_i^{(k)}$ is the shape factor that depends on the reference structure for atom i. Shape factors for various structures are specified in the work of Baskes[9]. The par-

tial electron densities are given by

$$\rho_i^{(0)} = \sum_{j\neq i} \rho_j^{a(0)}(r_{ij})\, S_{ij} \tag{9a}$$

$$\left(\rho_i^{(1)}\right)^2 = \sum_{j\neq i}\left[\rho_j^{a(1)}\frac{r_{ij}}{r_{ij}} S_{ij}\right]^2 \tag{9b}$$

$$\left(\rho_i^{(2)}\right)^2 = \sum_{j\neq i}\left[\rho_j^{a(2)}\frac{r_{ij}\, r_{ij}}{r_{ij}^2} S_{ij}\right]^2 - \frac{1}{3}\left[\sum_{j\neq i}\rho_j^{a(2)}(r_{ij})\, S_{ij}\right]^2 \tag{9c}$$

$$\left(\rho_i^{(3)}\right)^2 = \sum_{j\neq i}\left[\rho_j^{a(3)}\frac{r_{ij}\, r_{ij}\, r_{ij}}{r_{ij}^3} S_{ij}\right]^2 - \frac{3}{5}\sum_{j\neq i}\left[\rho_j^{a(3)}\frac{r_{ij}}{r_{ij}} S_{ij}\right]^2 ; \tag{9d}$$

where r_{ij} is the component of the displacement vector from atom i to atom j. S_{ij} is the screening function between atoms i and j and is defined in Eqs. (16). The atomic electron densities are computed as

$$\rho_i^{a(k)}(r_{ij}) = \rho_{i0}\exp\left[\beta_i^{(k)}\left(\frac{r_{ij}}{r_i^0} - 1\right)\right] ; \tag{10}$$

where r_i^0 is the nearest-neighbor distance in the single-element reference structure and $\beta_i^{(k)}$ is element-dependent parameter. Finally, the average weighting factors are given by

$$t_i^{(k)} = \frac{1}{\rho_i^{(0)}}\sum_{j\neq i} t_{0;j}^{(k)}\, \rho_j^{a(0)} S_{ij}; \tag{11}$$

where $t_{0;j}^{(k)}$ is an element-dependent parameter.

The pair potential is given by

$$\phi_{ij}(r_{ij}) = \phi_{ij}(r_{ij})\, S_{ij} \tag{12}$$

$$\phi_{ij}(r_{ij}) = \frac{1}{Z_{ij}}\left[2E_{ij}^u(r_{ij}) - F_i\left(\frac{Z_{ij}}{Z_i}\rho_j^{a(0)}(r_{ij})\right) - F_j\left(\frac{Z_{ij}}{Z_j}\rho_j^{a(0)}(r_{ij})\right)\right] \tag{13}$$

$$E_{ij}^u(r_{ij}) = E_{ij}\left(1 + a_{ij}(r_{ij})\right) e^{-a_{ij}(r_{ij})} \tag{14}$$

$$a_{ij} = \beta_{ij}\left(\frac{r_{ij}}{r_{ij}^0} - 1\right) ; \tag{15}$$

where E_{ij}, β_{ij} and r_{ij}^0 are element-dependent parameters and Z_{ij} depends upon the structure of the reference system. The background densities $\hat{\rho}_i(r_{ij})$ in Eq. (13) are the densities for the reference structure computed with interatomic spacing r_{ij}.

The screening function S_{ij} is designed so that $S_{ij} = 1$ if atoms i and j are unscreened and within the cutoff radius r_c, and $S_{ij} = 0$ if they are completely screened or outside the cutoff radius. It varies smoothly between 0 and 1 for partial screening. The total screening function is the product of a radial cutoff function and three body terms involving all other atoms in the system:

$$S_{ij} = S_{ij} f_c\left(\frac{r_c - r_{ij}}{r}\right) \tag{16a}$$

$$S_{ij} = \prod_{k\neq i,j} S_{ikj} \tag{16b}$$

$$S_{ikj} = f_c\left(\frac{C_{ikj} - C_{min;ikj}}{C_{max;ikj} - C_{min;ikj}}\right) \tag{16c}$$

$$C_{ikj} = 1 + 2\frac{r_{ij}^2 r_{ik}^2 + r_{ij}^2 r_{jk}^2 - r_{ij}^4}{r_{ij}^4 - r_{ik}^2 - r_{jk}^2} \tag{16d}$$

$$f_c(x) = \begin{cases} 1 & x \geq 1 \\ \left[1 - (1-x)^4\right]^2 & 0 < x < 1 \\ 0 & x \leq 0 \end{cases} \tag{16e}$$

Note that C_{min} and C_{max} can be defined separately for each i-j-k triplet, based on their element types. The parameter r controls the distance over which the radial cutoff is smoothed from 1 to 0 near $r = r_c$.

III. DETERMINATION OF THE MEAM POTENTIAL PARAMETERS

A. MEAM potentials for pure Al and Mg system

The previously published MEAM parameters for Al[21] and Mg[9] served as the basis for the present work. For some of the surface and point defect calculations, however, we observed less than satisfactory agreement between DFT and the MEAM calculations when these original MEAM potential parameters were used. We followed similar procedures prescribed by Lee et al.[21] and Baskes[9] to fine-tune the parameters and improve the overall agreement with experiments and DFT calculations. For each element, several material parameters obtained from the reference structure are utilized to determine the model parameters. These materials parameters include the cohesive energy, equilibrium atomic volume, bulk modulus, and several elastic constants. The most stable crystal structures were chosen as the reference structures, namely a face-centered cubic (fcc) structure for Al and a hexagonal close packed (hcp) structure for Mg. The new parameters obtained from the present work are listed in Table I. The merits of these new potentials are demonstrated in various calculations described in Sec. IV.

TABLE I: Set of the MEAM potential parameters for pure Al and Mg. E_c is the cohesive energy, a_0 is the equilibrium lattice parameter, A is the scaling factor for the embedding energy, $$ is the exponential decay factor for the universal energy, $^{(0\ 3)}$ are the exponential decay factors for the atomic densities, $t^{(0\ 3)}$ are the weighting factors for the atomic densities, C_{max} and C_{min} are the screening parameters. The reference structures for Al and Mg are fcc and hcp, respectively.

Element	E_c [eV]	a_0 [Å]	A		$^{(0)}$	$^{(1)}$	$^{(2)}$	$^{(3)}$	$t^{(0)}$	$t^{(1)}$	$t^{(2)}$	$t^{(3)}$	C_{max}	C_{min}
Al	3.353	4.05	1.07	4.64	2.04	1.50	6.0	1.50	1.00	4.00	–2.30	8.01	2.8	2.0
Mg	1.55	3.20	1.11	5.45	2.70	0.0	0.35	3.0	1.00	8.00	4.10	–2.00	2.8	2.0

TABLE II: The MEAM potential parameters for the Mg-Al alloy system. E_c is the cohesive energy, r_e is the equilibrium nearest neighbor distance, $$ is exponential decay factor for the universal energy, C_{max} and C_{min} are screening parameters, $_0$ is the density scaling factor.

Parameter	Value
E_c [eV]	$(E_c^{Al} + E_c^{Mg})/2 \quad 0.4575$
r_e [Å]	2.821
	4.915
C_{min} (Al–Mg–Al)	0.0
C_{min} (Mg–Al–Mg)	2.0
C_{min} (Al–Al–Mg)	2.0
C_{min} (Al–Mg–Mg)	2.0
C_{max} (Al–Mg–Al)	2.8
C_{max} (Mg–Al–Mg)	2.8
C_{max} (Al–Al–Mg)	2.8
C_{max} (Al–Mg–Mg)	2.8
$_0$ (Al)	1.0
$_0$ (Mg)	0.6

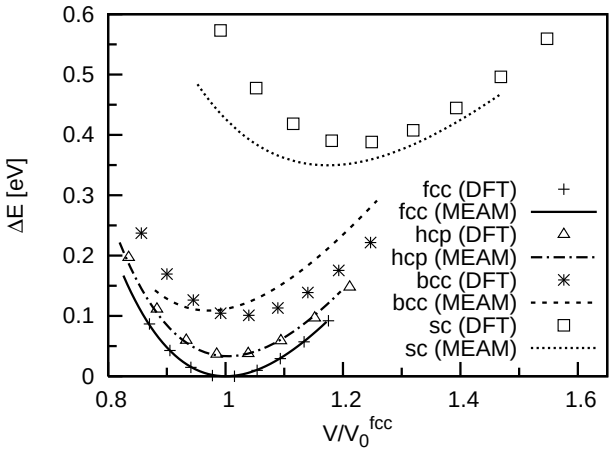

FIG. 1: Atomic energies (total energies per atom) as a function of the atomic volume (volume per atom) for Al atoms in fcc, hcp, bcc and simple cubic (sc) crystal structures. The energies are measured from the equilibrium atomic energy of fcc structure. Volumes are scaled by the equilibrium atomic volume of the fcc structure V_0^{fcc}.

B. MEAM potential for the Mg–Al alloy system

The parameters of the MEAM potential for the Mg-Al alloy system were determined from a procedure similar to the one prescribed by Lee[33]. The parameters were constructed to fit the elastic properties obtained from the DFT calculations for MgAl in the rock-salt (B1) structure, which was chosen to be the reference structure. The new parameters obtained from the present work are listed in Table II. Primary emphasis was put on matching the equilibrium volume and the bulk modulus, which were reproduced exactly (see Table III).

IV. VALIDATION OF MEAM POTENTIALS

We demonstrate the validity and the transferability of the new MEAM potentials by performing simulations on Al and Mg atoms in a variety of structural arrangements.

A. Bulk

1. Pure Al and Mg system

To test the validity of the MEAM potentials for single elements, each element was put into fcc, hcp, body-centered cubic (bcc), and simple cubic (sc) crystal structures. The atomic energies for several atomic volumes near equilibrium atomic volume were calculated. The results were compared with those of DFT calculations, as shown in Fig. 1. As expected, the curve for the fcc structure produced by the MEAM potential retraces the results of DFT calculations nearly perfectly since fcc was used as the reference structure during the potential construction process. The agreement between the MEAM potential and DFT for the hcp structure is also remarkable. The most important result, however, is the fact that the new MEAM potential correctly identified fcc as the most stable structure for Al. Furthermore, the sequence of the structures is correctly predicted in the order of stability by the new Al MEAM potential. The relative cohesive energies, with respect to the one for the fcc structure, are also in good agreement with the DFT calculations, although the result for the simple cubic structure is

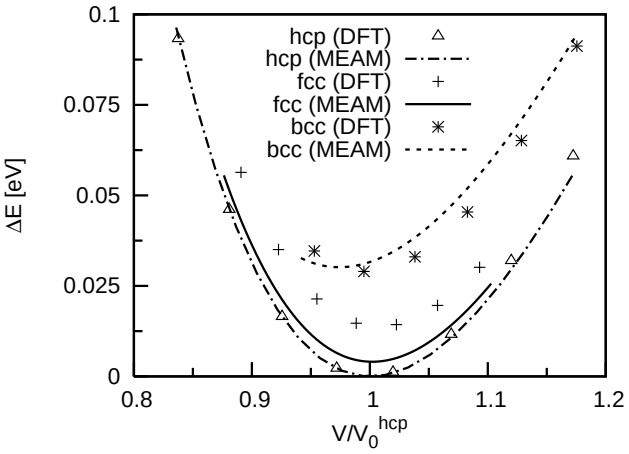

FIG. 2: Atomic energies of Mg as a function of the atomic volume in fcc, hcp, and bcc cubic crystal structures. The energies are measured from the equilibrium atomic energy of the hcp structure. Volumes are scaled by the equilibrium atomic volume of the hcp structure V_0^{hcp}.

slightly underestimated. The relative equilibrium atomic volumes, with respect to the one for the fcc structure, are also well reproduced. We point out that the equilibrium atomic volume for fcc Al, obtained by the MEAM potential (16.61A^3), is slightly different from the one predicted by DFT (15.76A^3). This is due to the fact that the MEAM parameters are fitted to reproduce the experimental volume, while DFT within LDA tends to underestimate the equilibrium lattice constants by roughly 1% (see, e.g. Ref. 34).

Fig. 2 shows the atomic energy plot for Mg atoms in different crystal structures compared with the results of the DFT calculations. The hcp structure was used as the reference structure for the Mg MEAM potential, and the DFT data points for this structure are accurately reproduced. The sequence of the structures is again predicted correctly in the order of stability by the new Mg MEAM potential. The relative atomic energies, with respect to the one for the hcp structure, are also in good agreement with the DFT calculations. Note that the scale of the vertical axis of Fig. 2 is six times larger than that of Fig. 1, and that the largest error in relative atomic energies (fcc case) is in the order of 0.01 eV. Similar to the Al potential, equilibrium atomic volume for hcp Mg in the MEAM is set to the experimental value of 23.16A^3, while DFT predicts a smaller value of 21.54A^3. Both the MEAM and the DFT methods prefer c=a ratio close to 0.994 of the ideal c=a ratio.

2. Mg-Al alloy system

To compare Mg-Al alloy systems with different stoichiometric coefficients, we define the heat of formation per atom as

$$H_f = \frac{E_{tot} - N_{Mg}\varepsilon_{Mg} - N_{Al}\varepsilon_{Al}}{N_{Mg} + N_{Al}}; \qquad (17)$$

where E_{tot} is the total energy of the system, N_{Mg} and N_{Al} are the numbers of Mg and Al atoms in the system, ε_{Mg} and ε_{Al} are the total energies per atom for Mg and Al in their ideal bulk structures, respectively. Table III lists some of the material properties the new MEAM potential reproduces for a MgAl compound in a B1 structure compared with the predictions of the DFT calculations. Due to our emphasis on the first three properties during the construction process, the last two columns show some discrepancies between the MEAM and DFT results.

TABLE III: Elastic parameters for MgAl in a B1 structure from the MEAM and DFT calculations. The units of the heat of formation per atom H_f and the equilibrium atomic volume V_0 are eV and A^3, respectively. The units of the bulk modulus B_0 and all elastic constants C_{ij} are GPa.

Method	H_f	V_0	B_0	C_{44}	$(C_{11} - C_{12})/2$
DFT	0.4575	22.4	38.4	39.1	40.6
MEAM	0.4575	22.4	38.4	14.3	29.8

Fig. 3 shows the heat of formation per atom H_f for the B1, B2 and B3 structures compared with the results from the DFT calculations. The B1 (cubic rock salt) structure was used as the reference structure for the Mg-Al alloy MEAM potential. Fig. 3 shows that the reference structure is not the most stable structure in Mg-Al binary systems. Again, the sequence of the structures in the order of stability is predicted correctly by the new MEAM potential for the Mg-Al alloy system. The relative cohesive energies, with respect to the one for the reference structure, are also in good agreement with the DFT calculations. The equilibrium atomic volume and bulk modulus of Mg-Al in the B1 structure are reproduced almost exactly. Note that the abscissa of the plot in Fig. 3 is the actual volume instead of the volume ratio used in Fig. 1 and Fig. 2.

To further demonstrate the validity of our new potentials, we also computed the heat of formation per atom for many intermetallic phases of Mg-Al alloys. The total energy values in Eq. 17 of B1, B2, B3, C1, C3, C9, C15, $D0_3$, $D0_9$, A15, $L1_2$ and A12 structures were evaluated at the optimal atomic volume for each structure. The results from the MEAM calculations, compared with the ones from the DFT calculations, are summarized in Fig. 4. Although the Mg and Al atoms in these intermetallic phases are in a chemical environment very different from the one in the reference structure (B1), the agreement between MEAM and DFT is quite satisfactory. In most cases, MEAM preserves the order of stability predicted by DFT. The differences in the heat of formation per atom from MEAM and DFT are less than 0.5 eV at most. However, we note that the MEAM failed to predict that the formation of one of the experimen-

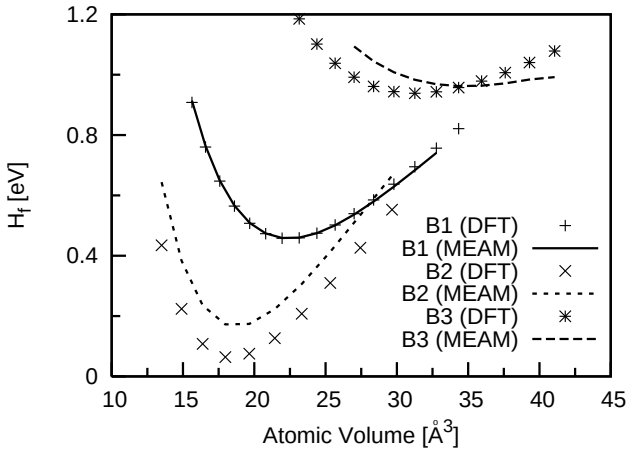

FIG. 3: The heat of formation per atom for MgAl alloys in the B1, B2 and B3 crystal structures.

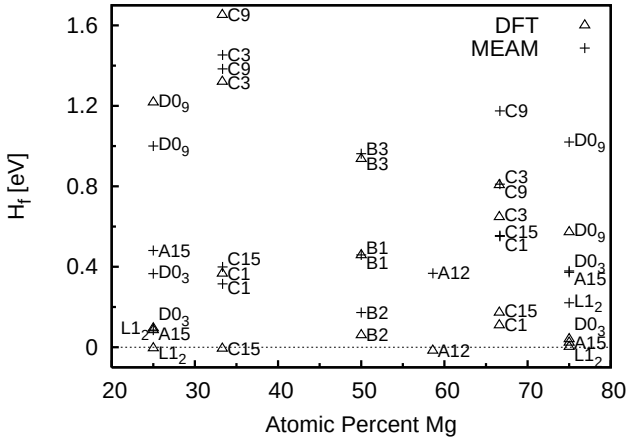

FIG. 4: The heat of formation per atom for Mg-Al alloys in various intermetallic phases with different stoichiometric coefficients. The results obtained from the new Mg-Al MEAM potentials are compared with the DFT calculations. The structure names are written next to the symbols (open triangles for DFT and crosses for MEAM).

tally observed Mg-Al alloy structures[35,36], ($Mg_{17}Al_{12}$) denoted as the A12 structure in Fig. 4, as an exothermic process. In comparison, our DFT calculation correctly predicted the H_f for this structure to be a negative value (-0.017 eV).

B. Surfaces

1. Surface formation energies

Semi-infinite surface is one of the simplest forms of defects. To test the transferability of the new MEAM potentials, surface formation energies for several different surfaces are computed. Surface formation energy per unit surface area E_{surf} is defined as

$$E_{surf} = (E_{tot} - N\varepsilon)/A; \quad (18)$$

where E_{tot} is the total energy of the structure with a surface, N is the number of atoms in the structure, ε is the total energy per atom in the bulk, and A is the surface area. Table IV shows the surface formation energies of many different surfaces constructed from fcc Al and hcp Mg crystals. Results from the present MEAM potentials are in good agreement with the DFT calculations, representing a significant improvement over two of the previously published MEAM potentials[21,22]. However, our MEAM potentials and the EAM potentials by Liu et al.[24] exhibit comparable levels of validity: our new MEAM potentials perform better for Mg surfaces while Liu's EAM potentials give better agreement for Al surfaces.

TABLE IV: Surface formation energies for fcc Al and hcp Mg. The units are mJ/m^2. The second column indicates if the structure was relaxed. Comparisons with other previously developed MEAM potentials are also given.

Surface	Relaxed	MEAM[a]	DFT	Others		
				Ref. 21	Ref. 22	Ref. 24[b]
Al(111)	No	737	992			913
Al(111)	Yes	731	988	629		912
Al(110)	No	1068	1371			1113
Al(110)	Yes	1035	1349	948		1107
Al(100)	No	1025	1213			1012
Al(100)	Yes	1025	1212	848		1002
Mg(0001)	No	604	638			500
Mg(0001)	Yes	595	637		310	499
Mg(1010)	No	642	855			517
Mg(1010)	Yes	523	846		316	515

[a] The present MEAM potential.
[b] Calculated using EAM parameters extracted from Ref. 24.

2. Stacking fault energies

Stacking fault is another kind of structure that occurs frequently in real materials and provides a good test environment for newly developed semiempirical potentials. Stacking fault energy per unit area is defined by

$$E_{sf} = (E_{tot} - N\varepsilon)/A; \quad (19)$$

where E_{tot} is the total energy of the structure with a stacking fault, N is the number of atoms in the system, ε is the total energy per atom in the bulk, and A is the unit cell area that is perpendicular to the stacking fault.

For Al, three stacking fault types from Hirth and Lothe[37] were examined and the results are listed in Table V. For the case of stacking fault type I, our MEAM result is in a good agreement with the available experimental value, even though our DFT result is lower than the experimental value. In all cases considered, the

TABLE V: Stacking fault energies for Al. Results from the present MEAM and DFT calculations are compared. Stacking fault energies per unit area are given in mJ/m^2.

Element	Fault	Relaxed	MEAM (DFT)		Exp.[b]
			Present	Other[a]	
Al	I	No	150 (136)	169	
Al	I	Yes	146 (133)	142	140–160
Al	E	No	150 (135)	169	
Al	E	Yes	148 (133)	154	
Al	T	No	75 (62)	84	
Al	T	Yes	74 (61)	77	

[a] Calculated using EAM parameters extracted from Ref. 24.
[b] Experimental results from Ref. 37.
I = ABCBCABC
E = ABCABCBABCABC
T = ABCABCABACBACB

TABLE VI: Stacking fault energies for Mg. Results from the present MEAM and DFT calculations are compared. Stacking fault energies per unit area are given in mJ/m^2. Comparisons with other previously developed MEAM potentials are also given.

Element	Fault	MEAM[a]	EAM[b]	AMEAM[c]	DFT[d]	DFT[e]
Mg	I_1	7	27	4	(18)	(20.9)
Mg	I_2	15	54	8	(37)	(43.7)
Mg	T_2	15	54	{	(45)	(51.3)
Mg	E	22	81	12	(61)	(68.1)

[a] The present MEAM potential.
[b] Calculated using EAM parameters extracted from Ref. 24.
[c] AMEAM results in Ref. 22
[a] DFT results from the present study.
[e] DFT results in Ref. 38
I_1 = ABABABCBCBCB
I_2 = ABABABCACACB
T_2 = ABABABCBABAB
E = ABABABCABABAB

present MEAM potentials shows better overall agreements with DFT calculations compared with the EAM potential by Liu et al.[24].

For Mg, four stacking fault types from the calculation of Chetty and Weinert[38] were examined. Total energy calculations for I_1, I_2, T_2, and E stacking fault types were performed using both DFT and MEAM calculations. The results are compared in Table VI. The present MEAM potential shows a substantial improvement over the previously published MEAM potential by Hu et al.[22]. The stacking fault energies are consistently underestimated by the present MEAM potentials compared to the results of the DFT calculations, while the results by the EAM potential from Ref. 24 are consistently overestimated.

TABLE VII: Adsorption energies E_{ads} and optimized height above the surface from MEAM calculations. Results from DFT calculations are given in parentheses. Units are eV and Å for energies and heights, respectively.

Surface	Adatom (site)	E_{ads}	Height
Al(111)	Al (hcp)	−2.64 (−3.29)	2.19 (2.05)
Al(111)	Al (fcc)	−2.67 (−3.26)	2.17 (2.08)
Al(111)	Mg (hcp)	−1.70 (−1.09)	2.46 (2.35)
Al(111)	Mg (fcc)	−1.70 (−1.07)	2.47 (2.35)
Mg(0001)	Al (hcp)	−2.17 (−2.68)	2.11 (2.16)
Mg(0001)	Al (fcc)	−2.17 (−2.68)	2.09 (2.14)
Mg(0001)	Mg (hcp)	−1.43 (−0.81)	2.17 (2.28)
Mg(0001)	Mg (fcc)	−1.49 (−0.82)	2.37 (2.27)

3. Adsorption on surfaces

The adsorption energy of a single adatom E_{ads} is given by

$$E_{ads} = E_{tot} - E_{surf} - E_{atom}; \qquad (20)$$

where E_{tot} is the total energy of the structure with the adatom adsorbed on the surface, E_{surf} is the total energy of the surface without the adatom, and E_{atom} is the total energy of an isolated atom. We placed single Al and Mg atoms at the fcc and hcp sites (see, e.g., Lvvik and Olsen[39] for the definition of these sites) on Al(111) and Mg(0001) surfaces. The entire structures were then relaxed to determine the adsorption energies. The height of the relaxed adatom is measured from the farthest atom (the one least affected by the adsorption) in the top surface layer. Table VII shows the results obtained from the MEAM and DFT calculations. Even though there are small quantitative discrepancies, the qualitative agreement between these two sets of data is quite satisfactory. For instance, DFT calculations predict that on Al(111) surfaces the adsorption of the Al atoms (same kind) is stronger (bigger adsorption energies and shorter heights) than the adsorption of Mg atoms (different kind). On the other hand, DFT calculations predict that on Mg(0001) surfaces, the adsorption of the Mg atoms (same kind) is weaker (smaller adsorption energies and longer heights) than the adsorption of Al atoms (different kind). Both of these features are clearly demonstrated by the new MEAM potentials.

C. Point defects

1. Vacancy

The formation energy of a single vacancy E_f^{vac} is defined as the energy cost to create a vacancy:

$$E_f^{vac} = E_{tot}[N] - N\varepsilon; \qquad (21)$$

where $E_{tot}[N]$ is the total energy of a system with N atoms containing a vacancy and ε is the energy per atom

TABLE VIII: Calculated single vacancy properties. Single vacancy formation energy E_f^{vac} and formation volume $_v$ values are obtained from the relaxed structures containing single vacancies. Here $_0$ is the bulk atomic volume. All energy values are listed in eV. The results from the MEAM calculations are compared with the results from the DFT calculations given inside the parentheses.

Element	E_f^{vac}		$_v = _0$	
	Present	Others	Present	Others
Al	0.68 (0.67)	0.68[a], 0.68[b]	0.66 (0.76)	0.72[a], 0.61[b]
Mg	0.58 (0.82)	0.59[c], 0.87[b]	0.76 (0.75)	0.83[c], 0.88[b]

[a] MEAM results in Ref. 21
[b] Calculated using EAM parameters extracted from Ref. 24.
[c] AMEAM results in Ref. 22

TABLE IX: The formation energies of various kinds of interstitial point defects in Al and Mg. All energy values are given in eV. The results from the MEAM calculations are compared with the results from the DFT calculations given inside the parentheses.

Bulk (structure)	Interstitial (site)	MEAM (DFT)
Al (fcc)	Al (dumbbell)	2.32 (2.94)
Al (fcc)	Al (octahedral)	2.91 (3.06)
Al (fcc)	Al (tetrahedral)	3.14 (3.68)
Al (fcc)	Mg (octahedral)	2.77 (3.79)
Al (fcc)	Mg (tetrahedral)	5.09 (4.25)
Mg (hcp)	Mg (octahedral)	1.29 (2.36)
Mg (hcp)	Mg (tetrahedral)	1.53 (2.35)
Mg (hcp)	Al (octahedral)	2.13 (1.97)
Mg (hcp)	Al (tetrahedral)	2.79 (2.11)

in the bulk. Table VIII shows the formation energy of single vacancies for fcc Al and hcp Mg obtained from the MEAM and DFT calculations. The new MEAM potentials reproduced a DFT value for Al vacancy formation energy very well, although the value for Mg was estimated somewhat low. Furthermore, the present MEAM potentials reproduce the correct amount of reduction in volume due to the formation of a vacancy. This also represents a substantial improvement over the existing MEAM potentials.

2. Interstitial point defects

The formation energy of an interstitial point defect E_f^{int} is given by

$$E_f^{int} = E_{tot}[N + A] \quad E_{tot}[N] \quad "_A \qquad (22)$$

where $E_{tot}[N]$ is the total energy of a system with N (Mg or Al) atoms, $E_{tot}[N + A]$ is the total energy of a system with N atoms plus one atom of type-A (Mg or Al) inserted at one of the interstitial sites, and $"_A$ is the total energy per atom of type-A in its most stable bulk structure. Note that the inserted atom A can be the same type as the matrix, in which case the point defect becomes a so-called self-interstitial defect. Interstitial atom formation energies were calculated for Al and Mg at octahedral, tetrahedral, and dumbbell sites. Atomic position and volume relaxation were performed. The results of these calculations are listed in Table IX, to be compared with the results from the DFT calculations. DFT results are well reproduced in general. According to the present calculations, the most stable form of a self-interstitial defect for fcc Al crystal is a dumbbell along the [100] direction, in agreement with the DFT results and an experimental observation by Jesson et al.[40]. The new MEAM potentials, however, failed to reproduce the results of the DFT calculations for the self-interstitial defects in a hcp Mg crystal. Our new MEAM potential indicates that the octahedral site will be more stable than the tetrahedral site, while the DFT calculations predict that both sites will have nearly the same formation energies. In both of the heterogeneous interstitial defects, the new MEAM potentials produce the same relative stability of different interstitial sites with the DFT calculations. However, Table IX should not be used to predict the most stable interstitial defects; it was not the purpose of the present work to perform an exhaustive search to draw such conclusions.

TABLE X: The formation energies of substitutional point defects in Al and Mg. All energy values are given in eV.

Bulk (structure)	Substitute	MEAM (DFT)
Al (fcc)	Mg	0.38 (0.06)
Mg (hcp)	Al	0.55 (0.09)

3. Substitutional point defects

The formation energy of a substitutional point defect E_f^{sub}, in the case of the substitution of an Al atom with a Mg atom, is defined by

$$E_f^{sub} = E_{tot}[Mg_{Al}] \quad E_{tot}[Al_{Al}] \quad "_{Mg} + "_{Al} \qquad (23)$$

where $E_{tot}[Mg_{Al}]$ is the total energy of a system of Al atoms plus one Mg atom that replaced an Al atom, $E_{tot}[Al_{Al}]$ is the total energy of the original system of Al atoms without a defect, $"_{Mg}$ and $"_{Al}$ are the total energies per atom for Mg and Al in their ideal bulk structures. The formation energy of a substitutional point defect for other cases can be defined similarly. Table X shows the results of substitutional defect calculations using the MEAM potentials and the DFT method. The new MEAM potentials predict correctly that substituting a Mg atom in a hcp structure with an Al atom costs more energy than the reverse as indicated by the DFT results, although the formation energies in both cases are larger than the values from the DFT calculations.

D. Molecular dynamics simulations

To validate the new potentials for molecular dynamics simulations, we calculated the melting temperatures of pure Al and Mg crystals. We followed the procedure prescribed by Morris et al.[41] to establish co-existence of solid and liquid phases to determine the melting temperatures. We obtained 930 K for pure Al crystal, which is in excellent agreement with the experimental value of 933 K. For Mg crystal, however, the two-phase method did not give a satisfactory result: 530 K compared to the experimental value of 923 K. To compare with other potentials, we followed a single-phase method as described by Kim and Tomanek[42], in which the temperature is increased at a constant rate and the specific heat of the system is monitored. Using this method, we obtained 780 K as the melting temperature of Mg crystals. This result is comparable to 745 K obtained by Liu et al.[43] using an EAM potential and following a similar method to compute the melting temperature.

The difficulty in computing accurate melting temperatures for hcp metals, such as Mg, using semiempirical potentials is well documented[44]. We believe that this is related to a small energy difference between hcp and fcc structures in our MEAM potential for Mg (see Fig. 2) and instability of hcp structures in MEAM[45]. Further detailed investigation of this subject is beyond the scope of the present work and will be reported in separate papers.

V. CONCLUSIONS

In this study we developed a new set of MEAM potentials for Al, Mg and their alloy systems using first-principles calculations based on DFT. The validity and transferability of the new MEAM potentials were tested rigorously by calculating physical properties of the Mg–Al alloy systems in many different atomic arrangements such as bulk, surface, and point defect structures. The new MEAM potentials show a significant improvement over the previously published potentials, especially for the surface formation, stacking faults, and point defect calculations. The new Mg-Al alloy potentials, however, failed to predict the stability of the ($Mg_{17}Al_{12}$) alloy intermetallic phase, suggesting the need for further improvements.

VI. ACKNOWLEDGMENT

The authors are grateful to the Center for Advanced Vehicular Systems at Mississippi State University for supporting this study. Computer time allocation has been provided by the High Performance Computing Collaboratory (HPC^2) at Mississippi State University. This work has also been supported in part by the US Department of Defense under the CHSSI MBD-04 (Molecular Packing Software for ab initio Crystal Structure and Density Predictions) project (S.G.K.) and by the U.S. Department of Energy, Office of Basic Energy Sciences (M.I.B.).

Electronic address: kimsg@hpc.msstate.edu

[1] Q. Han, K. B. K., and V. Srinath, Philos. Mag. 84, 3843 (2005).
[2] A. Lou, J. Renaud, I. Nakatsugawa, and J. Plourde, JOM 47, 28 (1995).
[3] G. Pettersen, H. Westergen, R. Hoier, and L. O., Mater. Sci. Eng. A 207, 115 (1996).
[4] M. O. Pekguleryuz and M. M. Avedesian, in DGM Conference on Magnesium Alloys and Their Applications (Oberursel: DGM Informations-gesellschaft, Garmisch-Partenkirchen, Germany, 1992), p. 213.
[5] I. J. Polmear, in DGM Conference on Magnesium Alloys and Their Applications (Oberursel: DGM Informations-gesellschaft, Garmisch-Partenkirchen, Germany, 1992), p. 201.
[6] J. F. King, Creep Resistance of Mg-Based Alloys (Wolfsburg: Werkso Informationsgesellschaft, 1998), p. 37.
[7] M. I. Baskes, Phys. Rev. Lett. 59, 2666 (1987).
[8] M. I. Baskes, J. S. Nelson, and A. F. Wright, Phys. Rev. B 40, 6085 (1989).
[9] M. I. Baskes, Phys. Rev. B 46, 2727 (1992).
[10] M. I. Baskes and R. A. Johnson, Modell. Simul. Mater. Sci. Eng. 2, 147 (1994).
[11] M. S. Daw, Phys. Rev. B 39, 7441 (1989).
[12] M. S. Daw and M. I. Baskes, Phys. Rev. B 29, 6443 (1984).
[13] M. S. Daw and M. I. Baskes, Phys. Rev. Lett. 50, 1285 (1983).
[14] F. J. Cherne, M. I. Baskes, and P. A. Deymier, Phys. Rev. B 65, 024209 (2001).
[15] M. I. Baskes, J. E. Angelo, and C. L. Bisson, Modell. Simul. Mater. Sci. Eng. 2, 505 (1994).
[16] K. Gall, M. F. Horstemeyer, M. van Schilfgaarde, and M. I. Baskes, J. Mech. Phys. Solids. 48, 2183 (2000).
[17] B.-J. Lee and M. I. Baskes, Phys. Rev. B 62, 8564 (2000).
[18] H. Huang, N. M. Ghoniem, J. K. Wong, and M. I. Baskes, Modell. Simul. Mater. Sci. Eng. 3, 615 (1995).
[19] M. I. Baskes, Mater. Chem. Phys. 50, 152 (1997).
[20] M. I. Baskes, Mater. Sci. Eng. A 261, 165 (1999).
[21] B.-J. Lee, J.-H. Shim, and M. I. Baskes, Phys. Rev. B 68, 144112 (2003).
[22] W. Hu, B. Zhang, B. Huang, F. Gao, and D. J. Bacon, J. Phys.: Condens. Matter 13, 1193 (2001).

[23] W. Hu, H. Deng, X. Yuan, and M. Fukumoto, Eur. Phys. J. B 34, 429 (2003).
[24] X.-Y. Liu, P. Ohotnicky, J. Adams, C. Rohrer, and R. Hyland, Surface Science 373, 357 (1997).
[25] B.-J. Lee and J. W. Lee, Calphad 29, 7 (2005).
[26] G. P. Potirniche, M. F. Horstemeyer, G. J. Wagner, and P. M. Gullett, Int. J. Plast. 22, 257 (2006).
[27] D. M. Ceperley and B. J. Alder, Phys. Rev. Lett. 45, 566 (1980).
[28] J. P. Perdew and A. Zunger, Phys. Rev. B 23, 5048 (1981).
[29] D. Vanderbilt, Phys. Rev. B 41, 7892 (1990).
[30] G. Kresse et al., J. Phys. Cond. Matter 6, 8245 (1994).
[31] G. Kresse and J. Furthmuller, Phys. Rev. B 54, 11169 (1996).
[32] Y.-M. Kim, B.-J. Lee, and M. I. Baskes, Phys. Rev. B 74, 014101 (2006).
[33] B.-J. Lee, Acta Materialia 54, 701 (2005).
[34] R. D. King-Smith and D. Vanderbilt, Phys. Rev. B 49, 5828 (1994).
[35] S. D., S. C., M. L., and C. R.-H., Intermetallics 11, 373 (2003).
[36] H. Okamoto, J. Phase Eq. 19, 598 (1998).
[37] J. P. Hirth and J. Lothe, Theory of Dislocations (John Wiley and Sons Inc, New York, 1982), 2nd ed.
[38] N. Chetty and M. Weinert, Phys. Rev. B 56, 10844 (1997).
[39] O. M. Lvvik and R. A. Olsen, Phys. Rev. B 58, 10890 (1998).
[40] B. J. Jesson, M. Foley, and P. A. Madden, Phys. Rev. B 55, 4941 (1997).
[41] J. R. Morris, C. Z. Wang, K. M. Ho, and C. T. Chan, Phys. Rev. B 49, 3109 (1994).
[42] S. G. Kim and D. Tomanek, Physical Review Letter 72, 2418 (1994).
[43] X.-Y. Liu, J. B. Adams, F. Ercolessi, and J. A. Moriarty, Modelling and Simulation in Materials Science and Engineering 4, 004 (1996).
[44] D. Y. Sun, M. I. Mendelev, C. A. Becker, K. Kudin, T. Haxhimali, M. Asta, J. J. Hoyt, A. Karma, and D. J. Srolovitz, Phys. Rev. B 73, 024116 (pages 12) (2006).
[45] K. Mae, T. Nobata, H. Ishida, S. Motoyama, and Y. Hiwatari, Modelling and Simulation in Materials Science and Engineering 10, 205 (2002).